BIBECHANA
Vol. 23, No. 3, August 2026, 137–153

ISSN 2091-0762 (Print), 2382-5340 (Online)
Journal homepage: http://nepjol.info/index.php/BIBECHANA
Publisher: Dept. of Phys., Mahendra Morang A. M. Campus (Tribhuvan University), Biratnagar

Ionospheric F2-Layer response to sudden and gradual commencement geomagnetic storms over the European mid-latitude sector

Samyam Pudasaini[1], Binod Adhikari[2], Rohit Bhattarai[1]
Iva Kumari Lamichhane[1], Manghang Limbu[1], Pramod Kamal Kharel[1],
Aasis Bhandari[1], Pitri Bhakta Adhikari[1*]

[1]*Department of Physics, Tri-Chandra Multiple Campus, Ghantaghar, Kathmandu, Nepal.*
[2]*Department of Physics, St. Xavier's College, Maitighar, Kathmandu, Nepal.*

[*]Corresponding author: Email: pbadhikari09@gmail.com

Abstract

This paper investigates the effects of the geomagnetic storms of 25–27 September 2011, 16–18 March 2013, and 6–8 September 2015 over five mid-latitude stations located in Europe: Dourbes (Belgium), Fairford (United Kingdom), Moscow (Russia), Rome (Italy), and Roquetes (Spain), and performs a cross-correlation analysis of ionospheric and solar parameters during these storms. We observed the highest fluctuations in ionospheric variables during the main phase of the storms. In addition, there is strong evidence of pre storm enhancement occurring at least a few hours and more than 24 hours prior to the main phase of the geomagnetic storms. We found that the TEC and foF2 parameters have a strong dependence with latitude for the events with Sudden Storm Commencement (SSC) in mid-latitude regions. Relatively low TEC and foF2 is observed in the higher-latitude stations, in particular at Moscow, which is at the highest latitude among the five stations, because of a decrease in the $n(O)/n(N_2)$ *ratio throughout the storm event. However, for the event with gradual storm commencement, there is no evidence of such dependence. The high correlation of Symmetric-H and Auroral Electrojet indices with ionospheric parameters indicates that the coupling mechanism between magnetosphere and ionosphere produces intense electric field disturbances in the middle–low latitudes. The storms drive intense solar wind energy into the auroral and mid-latitude upper atmosphere. This triggers rapid fluctuations in electron density, enhanced Joule heating and particle precipitation. The F2 layer is uplifted by up to* $\sim$*200 km and TEC is enhanced by up to* $\sim$*200% as compared to the quiet time. Such disturbances degrade HF radio communication and GNSS positioning, increase satellite drag and induce geomagnetically induced currents (GICs) in ground level conductor systems like power transmission lines. So, the lead and lag relationships obtained in this work can be used to protect sensitive devices on the ground and in space.*

Keywords
Symmetric-H, auroral electrojet, foF2, hmF2, total electron content.

Article information
Manuscript received: May 17, 2026; Revised: August 28, 2026; Accepted: August 29, 2026
DOI: https://doi.org/10.3126/bibechana.v23i3.90311

1 Introduction

Geomagnetic storms are produced when the interplanetary magnetic field (IMF) B_z component turns southward, strengthens (IMF $B_z < -10$ nT), and remains southward for a substantial length of time (longer than ∼3 hr; [1, 2]). As this happens, a rapid increase of dayside merging processes occurs at the magnetopause. When IMF-B_z is strongly negative, open field lines are produced by day side merging between the IMF and the geomagnetic field which allow the passage of mass, energy and momentum from the solar wind to the Earth's magnetosphere. This results in more solar wind energy input into all regions of the earth–atmosphere system, resulting in a geomagnetic storm. Geomagnetic storms are an important space weather phenomenon that, apart from affecting ground and satellite-based technological and high-frequency communications systems, can severely affect the dynamics and structure of the Earth's entire thermosphere and ionosphere. The ionospheric response to a geomagnetic storm is called an ionospheric storm that describes the ionospheric variations due to geomagnetic disturbances. Geomagnetic activity observed at the Earth is generally attributed to the occurrence of Coronal Mass Ejection (CME) on the Sun and the associated interplanetary shock waves or corotating interaction regions (CIR) produced by high-speed solar wind streams in the interplanetary medium [3–7]. CMEs are expulsions of mass from the Sun and are generally associated with solar flares or prominences. Once launched from the Sun, CMEs travel through the interplanetary medium and, if directed toward the Earth, reach the Earth in 1–4 days, depending on their speed. Therefore, in order to predict the geo-effectiveness of CMEs, one needs to examine the solar data from near the surface of the Sun and follow them through to the Earth. This is facilitated by an examination of ground-based and space-based multi-instrument data sets.

The ionosphere is the layer of the atmosphere that lies between 60 km and 1000 km above the Earth's surface and has a great importance in high frequency (HF) and satellite communications because of its electrical and ionic structure. The ionization characteristics and electron density distribution vary according to the location on Earth, time, solar, geomagnetic and seismic effects. The ionosphere consists of three distinct layers, namely D, E, and F. The F layer is the most significant layer in the ionosphere and the central part has the greatest electron density. During day time the F layer splits into F1 and F2 layers. The F2-layer, having the highest electron density, is the most stable layer for HF communications and it has major importance in satellite communications [8]. The F2 region is considered the most difficult and anomalous ionospheric region to predict [9]. In order to model this region, several authors have used the F2 critical frequency (foF2) and the F2 region peak height (hmF2) parameters. These parameters depend on various geophysical parameters including local time, season, solar and geomagnetic activity conditions and are believed to describe the overall behavior of the F2 layer ([10–19], and references therein). A better understanding of the variability and modeling of foF2 and hmF2 parameters is crucial for the development of ionospheric prediction capabilities, improvements in existing ionospheric models, and for radio propagation studies. Studies have shown that there are strong disturbances induced in the F-region of the ionosphere during strong geomagnetic storms. These perturbations cause large enhancements and reduction of electron density at the F2 region described as positive and negative ionospheric storm effects respectively (see, e.g., [20–23]). The occurrence of positive and negative storm effects depends upon the latitude, local time, and phase of the storm [20]. The ionospheric variations can be determined from the total electron content (TEC) or from the critical frequency of the F2-layer (foF2), which is a direct measure of the peak electron density (NmF2) of the F2-region ionosphere. The positive ionospheric storms have a high density of electrons and negative storms contain a lower density when compared to a normal quiet day [24]. The total electron content (TEC) is used to measure these densities, and is a key variable used in data to record and compare the intensities of ionospheric storms.

The response of the ionosphere during storm time is still an active area of research. Blagoveshchensky and Sergeeva [25] studied the storm of 7–8 September 2017 using many instruments and showed that the disturbances in the F-region degrade HF propagation conditions. Imtiaz et al. [26] analyzed the response of the low and mid-latitude ionosphere during the same event of September 2017. They reported that the vertical TEC enhancements depend on longitude and are caused by the combined effect of the CME and the high-speed solar wind streams. Habarulema et al. [27] studied conjugate locations over the Europe–African longitude sector. They found that the TEC response is asymmetric in the two hemispheres, which is related to the changes in thermospheric composition. Atici and Sagir [28] used the rate of TEC index obtained from a global GNSS network to map the ionospheric irregularities during storm time in different latitude regions. Wang et al. [29] reported that the asymmetries of the mid-latitude ionosphere in the two hemispheres occur at the same time but with opposite sign, which is produced by composition, vertical drift and traveling ionospheric disturbances. Recently, Themens et al. [30] presented an overview of the extreme storm of May 2024, in which the storm enhanced density plumes lifted the ionospheric peak by 150–300 km and produced GNSS scintillation over a wide region. These studies show that the study of the mid-latitude and high-latitude ionosphere during storm time is still important.

Ground magnetometers measure the integrated effect of all these disturbed-time and also quiet-time ionospheric and magnetospheric currents. Geomagnetic indices like the disturbance storm time index (Dst) and Symmetric H-component (SYM/H) index mainly represent ring current intensity during geomagnetic storms [31–33], derived using the longitudinally distributed chain of low latitude ground-based magnetometers. SYM/H is the same as Dst, but it has a 1-minute temporal resolution, which is very useful to study short temporal variations during the geomagnetic disturbances. SYM/H is derived by first subtracting the main geomagnetic field due to internal geodynamic and external Sq-induced geomagnetic field variations and then averaging residual fields. Therefore, it is a good proxy for the longitudinally symmetric component of the ring current. SYM/H is an indication of storm ring current intensity and AE gives auroral substorm ionospheric current intensities. There are other important factors like disturbance dynamo and penetrative electric fields that affect the perturbations in the ionosphere. Disturbance dynamo refers to a mechanism that generates electrical currents between the magnetosphere and the high-latitude ionosphere during dynamic interactions between the solar wind and the earth's magnetosphere which further penetrates directly to lower latitude through the conducting ionosphere [34]. Although it is one of the processes that contribute to ionospheric disturbances during geomagnetic storms, we are trying to study the broader impact of geomagnetic storms on the ionospheric parameters without specifically isolating disturbance dynamo effects. Also, penetration electric fields are one of the major disturbance electric fields in the mid-latitude ionosphere during geomagnetic storms [35], but here we have analyzed ionospheric parameters during quiet periods to establish a baseline and identified variations that are specifically associated with storm-time conditions.

Even after all these studies, two questions are still not answered. First, the cause of the pre-storm enhancement, which is a positive ionospheric disturbance seen from a few hours to more than a day before the onset of the storm, is still an unsolved problem in ionospheric physics [36, 37]. Second, most of the earlier studies are done for a single event or for a single parameter, which is mostly TEC. Very few works have measured the time lag between all three F2-layer parameters (foF2, hmF2 and TEC) and both the SYM/H and AE indices. Also, storms with sudden commencement and storms with gradual commencement have not been compared using the same stations. This is the research gap which we have tried to fill in this work. The novelty of our work is that we apply the same normalized cross-correlation analysis, with time lags up to ±4500 minutes, to three intense storms of solar cycle 24 having different types of commencement, using the same five European mid-latitude ionosonde stations along with a quiet-time baseline during solar minimum. In this way we obtain the lead and lag times between the ionospheric parameters and the storm indices. We also obtain two stationary points in the correlation curves, which give statistical evidence of the pre-storm enhancement. The importance of this study is that these lead times, and the finding that hmF2 responds at almost zero lag, can be used in space weather early warning systems. Such systems protect HF communication, GNSS positioning, satellite operation and ground level infrastructure like power transmission lines, which are affected by geomagnetically induced currents.

In the present study we investigate the solar and interplanetary conditions that were specific to intense geomagnetic storms of 25–27 September 2011, 16–18 March 2013, and 6–8 September 2015 (minimum SYM/H < -130 nT) in order to understand the relationships between the solar indices and ionospheric parameters associated with intense geomagnetic storms.

2 Data and methodology

In this study we have used five ionosonde stations of the European mid-latitude region, which lie in five different countries. These are Dourbes (Belgium), Fairford (United Kingdom), Moscow (Russia), Rome (Italy) and Roquetes (Spain). These stations are chosen for three reasons. First, they form a chain in latitude from 40.8°N to 55.47°N within a narrow range of longitude, so the effect of latitude on the storm response can be studied properly. Second, all five stations were working continuously during all the events studied here, so there is no gap in the data. Third, all of them belong to the Global Ionosphere Radio Observatory (GIRO) network, so the instruments and the data processing are the same for all the stations. Figure 1 shows the map of the ionospheric stations used in this study, and Table 1 lists their URSI codes and geographic coordinates. The observed F2-layer parameters (foF2, hmF2, and TEC) in this study are obtained from the ionosondes located at Dourbes (50.1° N, 4.6° E; data temporal resolution 5 min), Fairford (51.7° N, 358.5° E; 15 min), Moscow (55.47° N, 37.3° E; 15 min), Rome

Table 1: Geographic coordinates of stations

S.N.	Station name	URSI code	Latitude (°N)	Longitude (°E)
1	Dourbes, Belgium	DB049	50.10	4.60
2	Fairford, United Kingdom	FF051	51.70	358.50
3	Moscow, Russia	MO155	55.47	37.30
4	Rome, Italy	RO041	41.80	12.50
5	Roquetes, Spain	EB040	40.80	0.50

(41.8° N, 12.5° E; 15 min), and Roquetes (40.8° N, 0.5° E; 5 min) during the geomagnetic storms on 25–27 September 2011, 16–18 March 2013, and 6–8 September 2015. In order to investigate the F2-layer behaviors during low solar activity, the data under geomagnetic quiet-conditions on 17–19 March 2017 are selected. The data are available at the Digital Ionogram Data Base (DIDBase, https://giro.uml.edu/didbase/). The modulation of solar wind (SW) and interplanetary magnetic field (IMF) components (B_x, B_y, and B_z) high-resolution (1 min) data were obtained from the OMNI Database (https://omniweb.gsfc.nasa.gov/form/omni_min.html).

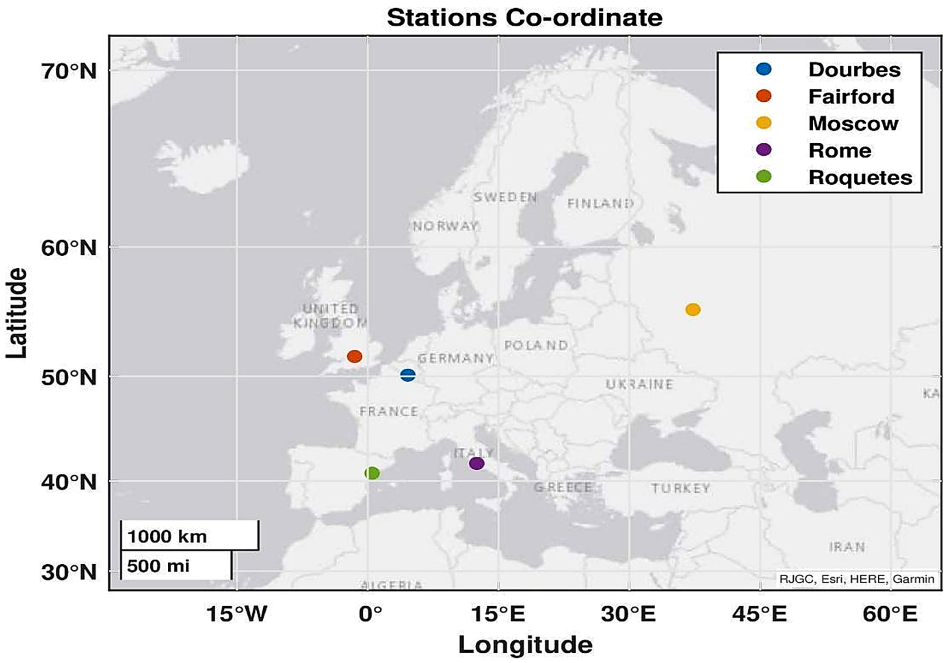

Figure 1: Map of the stations: Dourbes (Belgium), Fairford (United Kingdom), Moscow (Russia), Rome (Italy), and Roquetes (Spain).

The ionospheric parameters are measured by Lowell Digisonde Portable Sounder (DPS-4/DPS-4D) type digital ionosondes of the GIRO network [38]. These instruments sound the ionosphere by sweeping HF radio pulses over about 1–30 MHz. The ionograms recorded in this way are scaled automatically by the ARTIST software and are then checked manually by the observatories which operate the stations. This confirms the authenticity of the foF2, hmF2 and TEC values used here [39]. The interplanetary and geomagnetic data are taken from the OMNI database of NASA/GSFC. In this database the measurements of different spacecraft are cross-calibrated and are shifted in time to the bow shock nose of the Earth. Both DIDBase and OMNI are widely used and well validated data sets. The three storms of 2011, 2013 and 2015 are selected instead of more recent events for the following reasons. They are among the most intense and well separated storms of solar cycle 24, with minimum SYM/H < -130 nT for the SSC events. They also give a good comparison between two CME driven storms with sudden commencement and one storm with gradual commencement caused by a high-speed stream. Data of all five stations are available for all these events, and a quiet time baseline during solar minimum (17–19 March 2017) is also available near them. The aim of this work is to find the lead and lag relationship between the storm indices and the ionospheric parameters and not to report a particular recent event. So, the conclusions of this work do not depend on how recent the data are.

The sudden storm commencement (SSC) often serves as a reference time for the onset of a magnetic storm. The reliability of SSC for the storm onset has been argued for a long time. As a result, some investigators choose the main phase onset of the storm instead of SSC as the start time of a storm (e.g., [40]). Here we use SSC to indicate the onset of a magnetic storm for storms with a sudden commencement, except for the event on 6–8 September 2015 because it only had a gradual commencement. The SYM/H index is used to indicate the evolution and intensity of geomagnetic storms.

3 Results and discussion

3.1 Results

3.1.1 Event-1: 25–27 September 2011

Almost halfway through the ascending phase of the 24th solar cycle, a G2-level geomagnetic storm with Kp index of 6 occurred on 26 September 2011 due to a concentrated blast of electrically-conducting solar wind plasma and tangled magnetic field lines from region 1302 (N12E47) of the Sun. The region produced an X1.9 flare, an M7.1 long-duration X-ray flare and an M5.8 X-ray flare on 24 September (source: https://www.spaceweatherlive.com/).

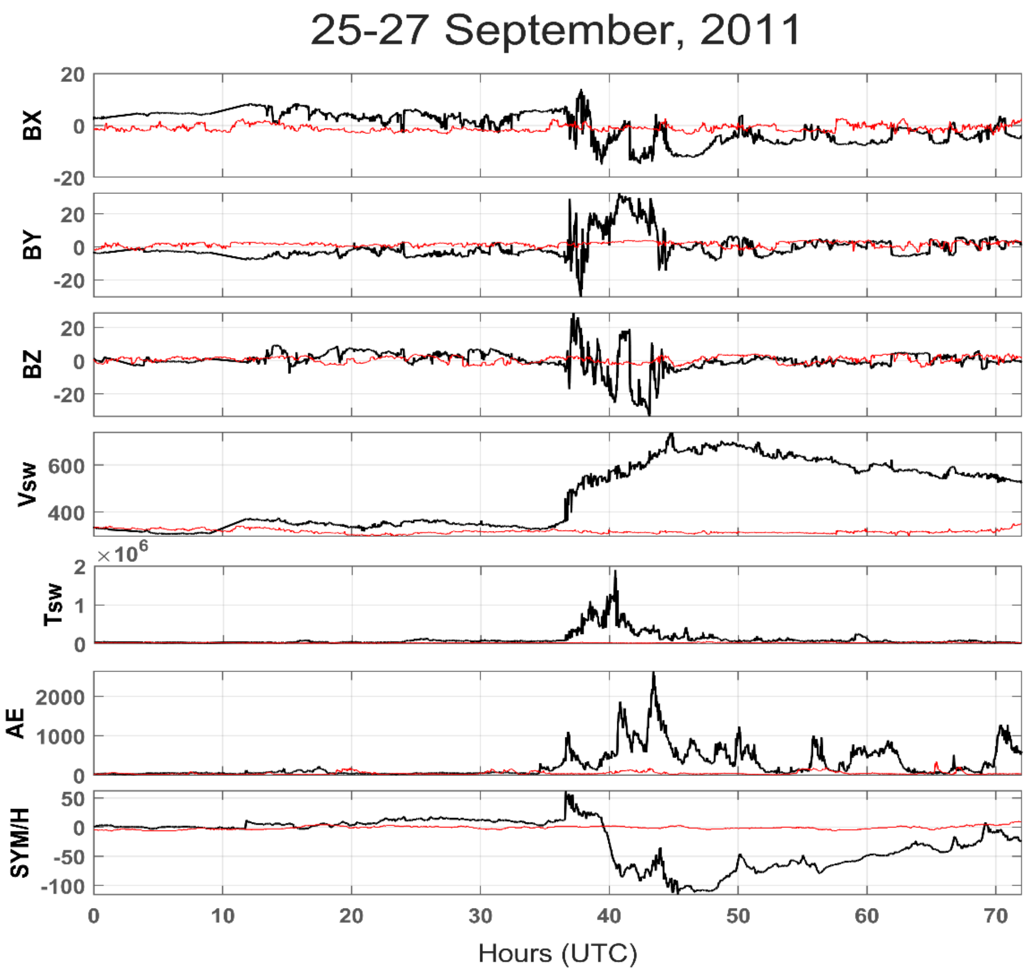

Figure 2: Variation in components of the magnetic field (in GSM coordinates), B_x (nT), B_y (nT) and B_z (nT), solar wind velocity V_{sw} (km/s), plasma temperature T_{sw} (K), geomagnetic indices, SYM/H (nT), and AE-index (nT) during the geomagnetic storm of 25–27 September 2011. The red curve denotes the variation during quiet days (18–20 March 2017).

Figure 2 displays the temporal evolution of interplanetary parameters B_x, B_y, B_z, solar wind velocity (V_{sw}), solar wind temperature (T_{sw}), geomagnetic activity indices AE (Auroral Electrojet) index, and SYM/H index for 25–27 September 2011. The differences between the various parameters during the event (indicated by black curves) and quiet days (indicated by red curves) are observed from the figure. At 12:38 (UTC) of 26 September the sudden storm commencement (SSC) is seen to have occurred when the symmetric horizontal component of the geomagnetic field SYM/H rose sharply from 15 nT to the highest point of 62 nT, indicating the beginning of the initial phase. During this period, all the ionospheric parameters significantly fluctuate while the north–south interplanetary magnetic field B_z altered between positive and negative values a few times with positive (negative) value indicating northward (southward) magnetic field, reaching its minimum of −33.61 nT at 19:07 (UTC) indicating a strong southward magnetic field. When the IMF B_z turns southward and becomes stronger, the auroral particle precipitation and the high latitude currents and convection are intensified. This causes enhanced Joule heating, ion-drag forcing, increased ionization at high latitudes and penetration of electric fields to low latitudes [41]. It can be observed that the minima in the B_z curve correlate well with the maxima in the AE index. At 19:27 (UTC), 20 minutes after B_z reached its minimum, the AE index reached its peak value of 2636 nT, which matches well with the result of [42]. Such a high AE index indicates that a large amount of energy is transferred into the magnetosphere from the solar wind [43]. The field components parallel to the ecliptic have no significant effect on substorms [44]. Also, when IMF-B_z becomes negative, the electric field linking the magnetosphere and the ionosphere increases [45]. The plasma flow speed started increasing from the initial phase throughout the main phase as was shown by [46] and reached its peak value of 738.6 km/s at 20:53 (UTC). Around this time the solar wind temperature had already cooled down, as it had reached its peak of 1.89×10^6 K earlier at 16:27 (UTC). The recovery phase started after SYM/H reached its lowest value of −113 nT at 20:54 (UTC).

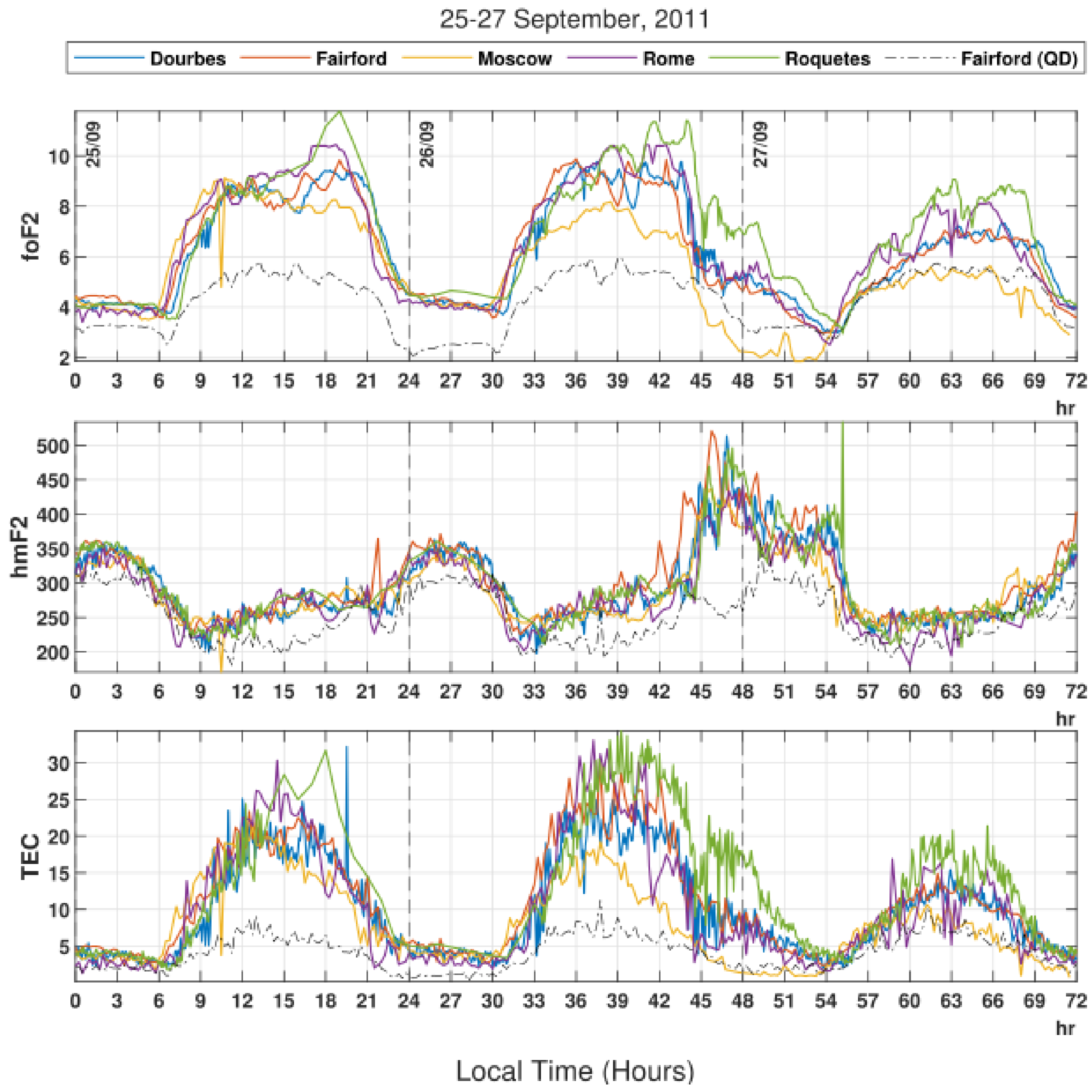

Figure 3: Changes in ionospheric parameters: F2-region critical frequency (foF2) in MHz, Total electron content (TEC) in ($\times 10^{16}$ m^{-2}), Maximum Ionization Height (hmF2) in km, recorded at stations Dourbes, Fairford, Moscow, Rome and Roquetes during the geomagnetic storm of 25–27 September 2011. The black curve denotes the variation during quiet days (18–20 March 2017).

Figure 3 depicts the variations of three different ionospheric parameters: F2-region critical frequency (foF2), maximum ionization height of F2-region (hmF2), and Total Electron Content (TEC) at five different stations: Dourbes, Fairford, Moscow, Rome and Roquetes. All the stations have similar variations because they all lie in the mid-latitude region. The daily variations of the day and night cycle can be easily noticed in all five stations. As the sun rises at around 06:30 local time, a sudden rise in foF2 and TEC is noticed in all the stations whereas around this time hmF2 is observed to have almost reached its lowest values around 09:00 (local time), indicating a negative correlation between them.

Relatively low TEC and foF2 are observed in Moscow, which is at the highest latitude among the five stations. This is because of a decrease in the $n(O)/n(N_2)$ ratio throughout the storm event [47]. The TEC and foF2 graphs clearly show latitudinal dependence, and the stations at Rome and Roquetes, being at the lowest latitudes, record the highest values of foF2 and TEC. This is similar to the results of [48] and [49]. The average of the highest critical frequency during the daytime of the 1st day is about ∼10 MHz, which is ∼100% higher than that of the quiet day. The mean highest TEC on the 1st day is $\sim 25 \times 10^{16}$ m^{-2}, which is ∼200% higher than that of the quiet day. This indicates that the positive storm had already started 1 day prior to the event day. Similar enhancements are seen throughout the main phase on 26 September, and they decrease in the recovery phase from 21:00 (local time). The occurrence of a positive storm before SSC is one of the unsolved problems in ionospheric research [36]. On the 1st day the maximum ionization height (hmF2) remains similar to that of the quiet day. During the main phase an increase in hmF2 is observed to be ∼50 km more in all stations. A sudden increase in hmF2 from ∼300 km to ∼450 km is observed at the beginning of the recovery phase, which is ∼200 km more than that of the quiet day. The plasma vertical drift getting increased by storm-induced circulation is the cause of the uplifting of the F2 layer [36]. Continuous substorm activity also enhances the equatorward winds, which may be another cause of this sudden increase [50]. The uplifting decreases and almost coincides with the quiet day on 27 September.

3.1.2 Event-2: 16–18 March 2013

A G3-class (Kp = 7) Earth-directed Coronal Mass Ejection (CME) event was observed on 17 March 2013, which is one of the strongest geomagnetic disturbances recorded during the 24th solar cycle with peak intensity of SYM/H ∼−132 nT. Figure 4 displays the temporal evolution of interplanetary parameters B_x, B_y, B_z, solar wind velocity (V_{sw}), solar wind temperature (T_{sw}), geomagnetic activity indices AE (Auroral Electrojet) index, and the symmetric horizontal component of the geomagnetic field (SYM/H) for 17–18 March 2013.

This storm was triggered by an Earth-directed coronal mass ejection [51] associated with an M1.1-type solar flare from the sunspot 1692 (N09W03) on 15 March 2013 at 07:00 UT. The incoming CME enhances the B_z (north–south) to strong northward and the solar wind speed rose to 600 km/s at around 06:00 UT on 17 March 2013, while the magnetic field components also vary significantly. The sudden enhancement of solar wind density and velocity because of the CME hitting the magnetosphere triggers the magnetopause current, which enhances our terrestrial magnetic field, which is registered as a sudden storm commencement (SSC) on SYM/H as shown in Figure 4. An immediate onset of intense auroral activity is seen in the AE index, reaching a magnitude as high as 2000 nT, indicating the generation of an energy source in the high-latitude region. The initial phase lasted for approximately one hour and the main phase began around 07:00 UT, as identified by the decrease in SYM/H implying the ring current intensification, and the SYM/H index reached a first minimum of around −110 nT around 10:00 UT on 17 March. Then it stayed nearly steady until it attained a second minimum of about −132 nT at ∼20:30 UT before recovery, which means that the main phase lasted for around 13 hours. The recovery phase lasted for more than 3 days as indicated by an increase in the SYM/H index. There is a directional discontinuity (DD) at ∼01:12 UT on 18 March (shown by a blue vertical line) clearly observed in the IMF components, solar wind temperature, and solar wind velocity. The IMF B_z turns northward after the directional discontinuity which contributes to a prompt magnetic storm recovery. This northward turning causes a cessation of auroral activity due to reduced dayside merging [52]. Directional discontinuities in Interplanetary Coronal Mass Ejections are an important factor in determining the geo-effectiveness of the event since they are characterized by sharp changes in coupling functions [53]. A gradual decrease in auroral activity and then a total cessation during the northward IMF interval is observed [54]. The SYM/H index is observed to recover completely after about 3 days. This geomagnetic storm is caused by the double action of southward IMF B_z in the sheath causing the storm onset and southward IMF B_z in the MC intensifying the storm.

Figure 5 shows the F2-layer parameters (foF2, hmF2, and TEC) between 16–18 March 2013. The top panel shows foF2, the middle panel shows hmF2, and the bottom panel shows TEC obtained from ionograms of Dourbes, Fairford, Moscow, Rome, and Roquetes. Similar to event 1, Moscow, being at higher latitude, has the lowest TEC and foF2 among the five stations, for reasons similar to those mentioned above in event 1, because of a decrease in the $n(O)/n(N_2)$ ratio throughout the storm event [47]. Latitude dependence can be observed in the graphs of TEC and foF2 as pointed out in [48] and [49]. Similarly, the ionosonde stations at Rome and Roquetes, being at the lowest latitudes, record the highest values of foF2 and TEC.

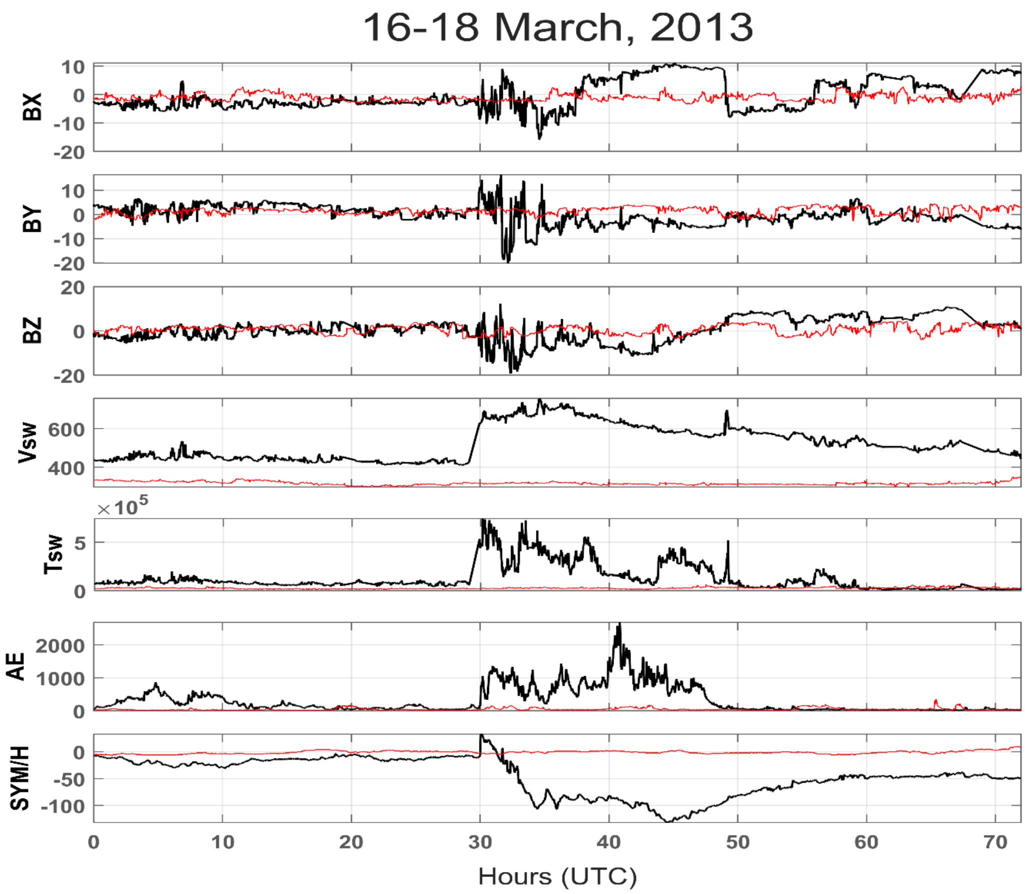

Figure 4: Variation in components of the magnetic field (in GSM coordinates), B_x (nT), B_y (nT) and B_z (nT), solar wind velocity V_{sw} (km/s), plasma temperature T_{sw} (K), geomagnetic indices, SYM/H (nT), and AE-index (nT) during the geomagnetic storm of 16–18 March 2013. The red curve denotes the variation during quiet days (18–20 March 2017).

The average of the highest critical frequency during the daytime of the 1st day is about ∼10 MHz, which is ∼100% higher than that of the quiet day. The mean highest TEC on the 1st day is $\sim 25\times10^{16}$ m^{-2}, which is ∼200% higher than that of the quiet day. The lowest values during the nighttime are also higher than those of the quiet day, being 5 MHz for foF2 and $\sim 5\times10^{16}$ m^{-2} for TEC. Here also the positive storm had already started 1 day prior to the event day. Similar enhancements remain throughout the main phase on 17 March and they decrease when the recovery phase starts at around 20:30 (local time). On 16 and 17 March the maximum ionization height (hmF2) shows only a slight increment. During the main phase an increase in hmF2 is observed to be ∼100 km more in all stations, and a sudden increase from ∼250 km to ∼350 km is observed at 11:00 (local time). On 18 March, hmF2 remained quiet throughout the day.

3.1.3 Event-3: 6–8 September 2015

An unforeseen powerful coronal hole solar wind stream sparked a moderate G2-class (Kp = 6) geomagnetic storm on 8 September 2015, with peak intensity of SYM/H −83 nT occurring at 02:00 UT on 8 September. Figure 6 shows the temporal evolution of solar wind parameters, the interplanetary magnetic field components B_x, B_y, B_z, solar wind velocity (V_{sw}), solar wind temperature (T_{sw}), AE index and SYM/H, from 6–8 September 2015. It can be inferred from the graph that there had been a pre-storm enhancement on 6–7 September, with solar wind parameters fluctuating repeatedly on those days. The incoming solar wind has triggered magnetic field components to vary significantly. These values oscillate to either side of the reference value for the B_y and B_z components during the event. However, the B_x component's value oscillates below the reference value till the recovery phase (02:00 UT, 8 September). Similarly, solar wind speed rose to 620 km/s at around 17:00 UT on 7 September. The sudden enhancement of solar wind density and velocity sets off the magnetopause current, represented by SYM/H as shown in Figure 6, which amplifies our terrestrial magnetic field [55]. Intense auroral activity is seen as the AE index reaches a magnitude as high as around 2800 nT at 16:00 UT on 7 September, indicating the generation of energy sources in the high-latitude region. Likewise, T_{sw} rose 2 hrs prior to the event, which might be due to the pre-storm effect. However, the temperature of the solar wind before the storm disturbance is found to be higher than during the main phase (MP) of the event, indicating pre-storm phenomena [56].

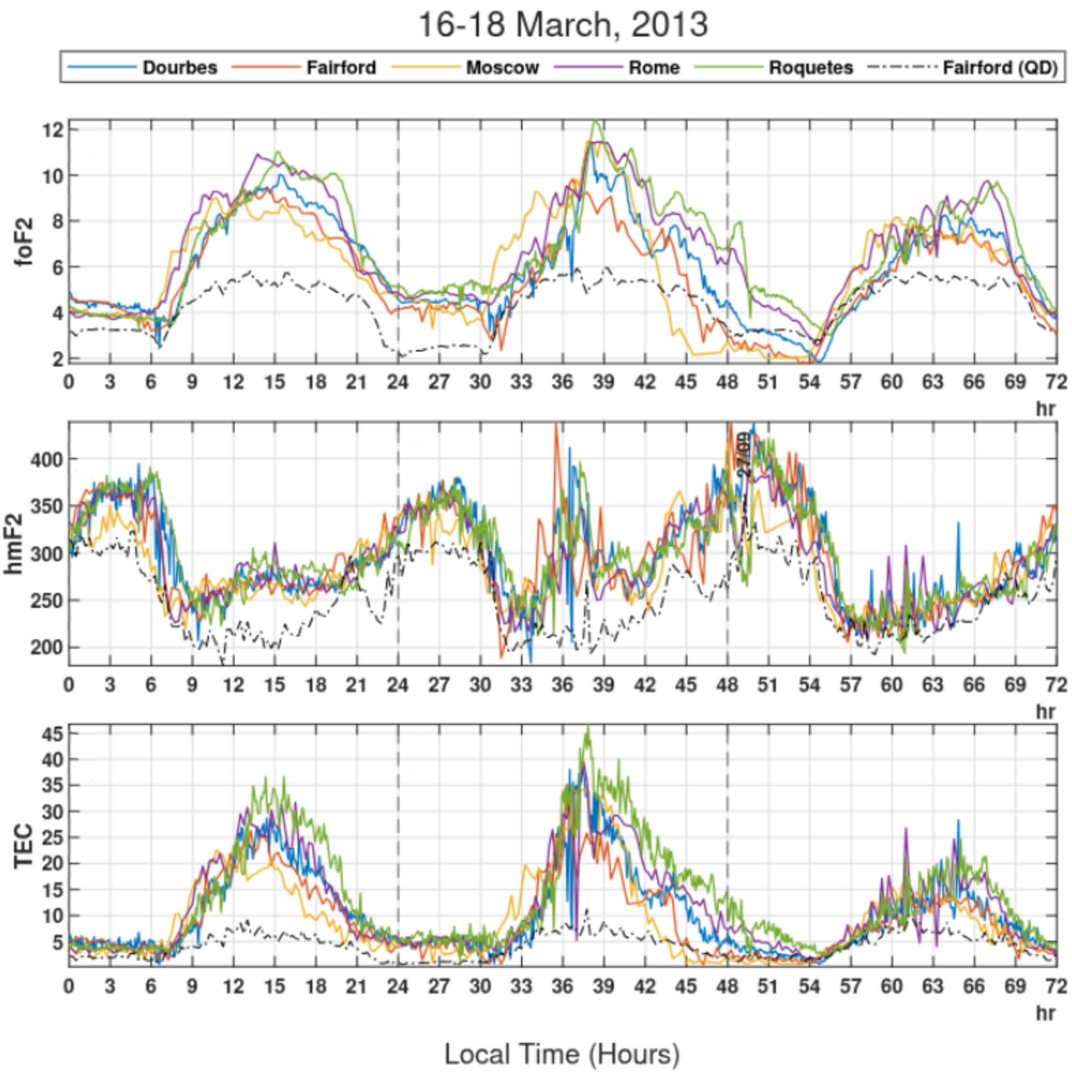

Figure 5: Change in ionospheric parameters, F2-region critical frequency (foF2) in MHz, Total electron content (TEC) in ($\times 10^{16}$ m^{-2}), Maximum Ionization Height (hmF2) in km, recorded at stations Dourbes, Fairford, Moscow, Rome and Roquetes during the geomagnetic storm of 16–18 March 2013. The black curve denotes the variation during quiet days (18–20 March 2017).

Values of the ionospheric parameters foF2, hmF2 and TEC of the five different stations during the 2015 geomagnetic storm are plotted in Figure 7. As we have chosen all the stations lying in the mid-latitude region, the variation of the parameters is almost the same for all stations. The value of foF2 increases slightly during the main decreasing phase of SYM/H and decreases during its increasing phase. foF2 in Roquetes has its peak value of 8.7 MHz at 19:25 LT (7 September), which is about 3.5 MHz more than in quiet days. During the main phase, the maximum increase in hmF2 is observed to be ∼205 km more at the Fairford station as compared to the quiet day. The increase in hmF2 is observed to be only ∼135 km in the Rome and Moscow stations, and there is only a slight increase at the Roquetes and Dourbes stations. The plasma vertical drift getting increased by storm-induced circulation is the cause of the uplifting of the F2 layer [36]. The spikes on the graph decrease and almost coincide with the quiet day in the later hours of 8 September. The maximum value of TEC during the main phase is $\sim 40 \times 10^{16}$ m^{-2}, which is about 32 units more than in quiet days, whereas during the recovery phase its value decreases to $\sim 27 \times 10^{16}$ m^{-2}. This increase of TEC during the main phase is due to auroral activity, the influx of plasma and the seasonal effect, as TEC content is highest during the equinox seasons [57]. The TEC and foF2 graphs do not show any latitudinal dependence, which contradicts the result shown by [48] and [49].

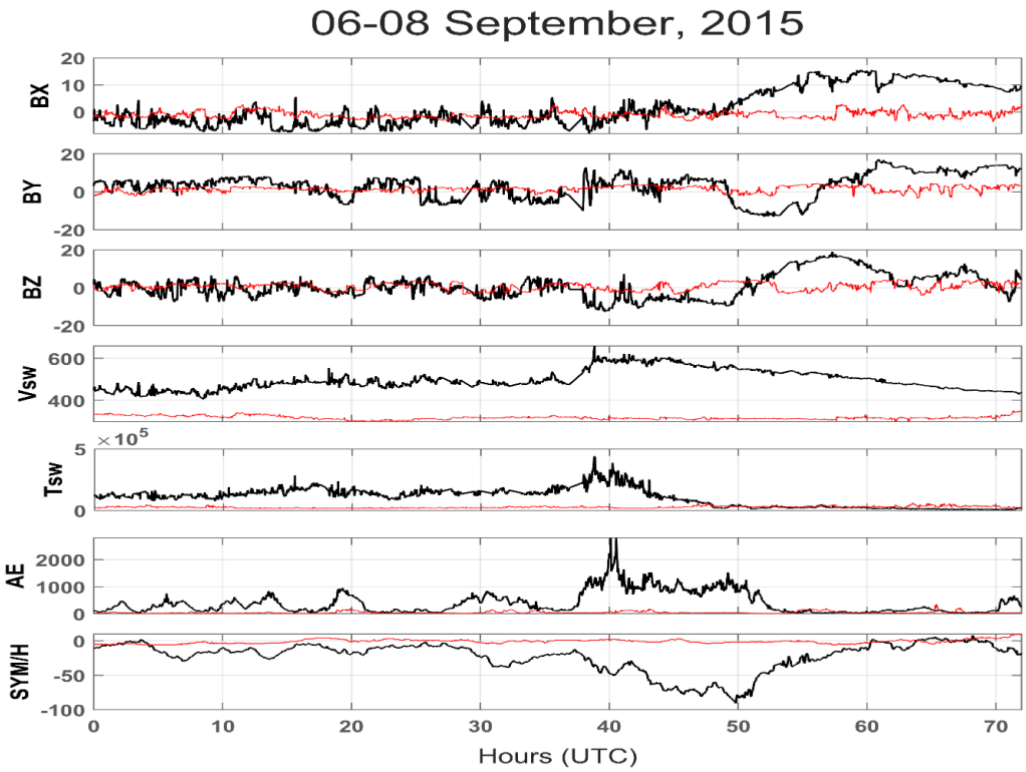

Figure 6: Variation in components of the magnetic field (in GSM coordinates), B_x (nT), B_y (nT) and B_z (nT), solar wind velocity V_{sw} (km/s), plasma temperature T_{sw} (K), geomagnetic indices, SYM/H (nT) and AE-index (nT) during the geomagnetic storm of 6–8 September 2015. The red curve denotes the variation during quiet days (18–20 March 2017).

3.1.4 Cross-correlation analysis

For all the cross-correlation analyses shown in this paper, the y-axis represents the normalized correlation coefficients and the x-axis represents the time lag. Each unit in the x-axis is equivalent to a time lag of 15 minutes, and the range is from −4500 to +4500 minutes. In all cases the ionospheric parameter is kept fixed and copies of the solar storm indices are shifted (lagged). The correlation coefficient at each point of lag is calculated, normalized and plotted in the graph. Figure 8 shows the analysis with SYM/H and Figure 9 shows the analysis with the AE index. The average of the highest values and their time lags are given in Table 2.

In the top block of Figure 8, the cross-correlation between TEC and SYM/H is analyzed. For the two events with SSC, the maximum anti-correlation is not observed at one point only but at two different points. In 2011 these two points are at time lags of −1878 minutes (1 day 7 hours and 18 minutes) and −450 minutes (7 hours and 30 minutes). In 2013 they are at −1623 minutes (1 day 3 hours and 3 minutes) and −300 minutes (5 hours). But for the event of 2015, which has gradual commencement, only one minimum is observed, with an average correlation of −0.736 at a time lag of −492 minutes (8 hours and 12 minutes). The quiet day shows only a moderate anti-correlation with a lag of about 7 hours. Hence, at least 5 hours of lead in the variation of total electron content is observed when compared with the SYM/H index. Almost equal evidence of TEC leading SYM/H by just more than one day is also obtained from the analysis. This explains the occurrence of a positive storm 1 day prior to the sudden storm commencement. The middle block shows the analysis between foF2 and SYM/H, and the same pattern is seen here. In 2013, foF2 leads SYM/H by −60 to −285 minutes with correlations up to −0.80, and a second minimum is again seen at a lead of more than a day. In 2015 an average correlation of −0.734 is observed at a lag of −408 minutes (6 hours 48 minutes). The bottom block shows the analysis between hmF2 and SYM/H, and here the result is different. The highest anti-correlation is observed at zero lag, being −0.795 in both 2013 and 2015. This shows that the maximum ionization height responds along with the ring current and not before it.

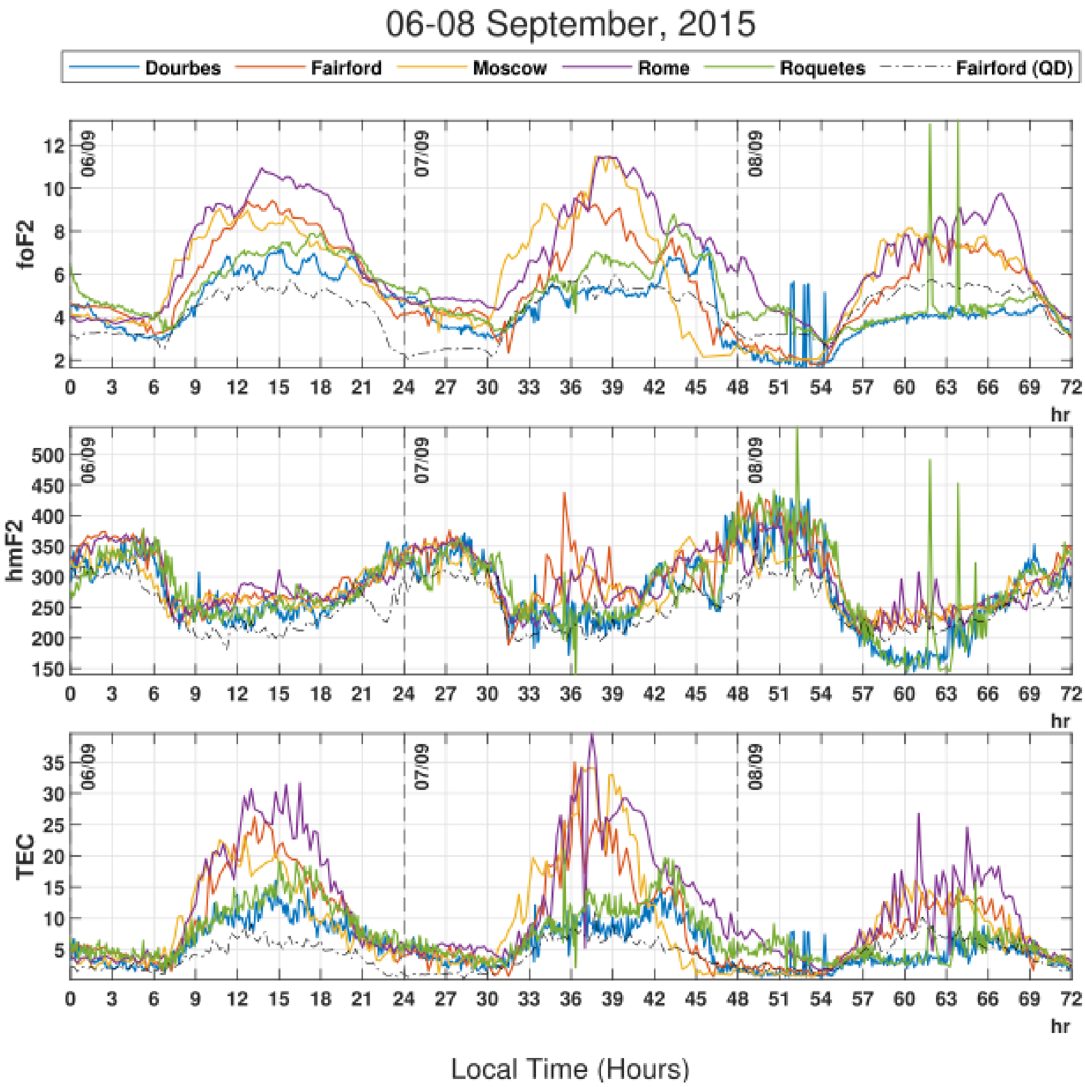

Figure 7: Change in ionospheric parameters, F2-region critical frequency (foF2) in MHz, Total electron content (TEC) in ($\times 10^{16}$ m^{-2}), Maximum Ionization Height (hmF2) in km, recorded at stations Dourbes, Fairford, Moscow, Rome and Roquetes during the geomagnetic storm of 6–8 September 2015. The black curve denotes the variation during quiet days (18–20 March 2017).

Figure 9 shows the cross-correlation of the same parameters with the AE index, and the results are similar but with positive correlation. TEC and foF2 lead the AE index from nearly zero up to a few hours. For example, in 2015 the highest correlation of TEC with AE is 0.749 at a lag of −17.6 units, and that of foF2 with AE is 0.65 at a lag of −14.4 units. A second and weaker maximum is again observed at a lead of more than 24 hours. This second maximum is highest for Moscow in the event of 2011, which indicates a strong pre-storm effect in the station at the highest latitude during the event caused by the most intense flare (X1.9). Like the case of SYM/H, hmF2 correlates with the AE index at nearly zero lag, the difference being only about ±2 hours depending upon the type of storm. The two stationary points obtained at the same time lags in all the analyses of TEC and foF2

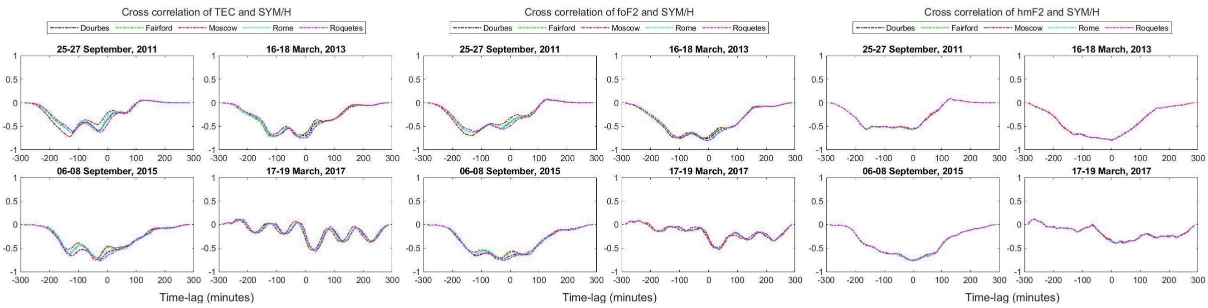

Figure 8: Cross-correlation of the ionospheric parameters with SYM/H: TEC & SYM/H (top), foF2 & SYM/H (middle) and hmF2 & SYM/H (bottom). In each block the panels are the storms of 25–27 September 2011 (1st), 16–18 March 2013 (2nd), 6–8 September 2015 (3rd) and the quiet days 18–20 March 2017 (4th). The x-axis is time lag (1 unit = 15 min); the y-axis is the correlation coefficient.

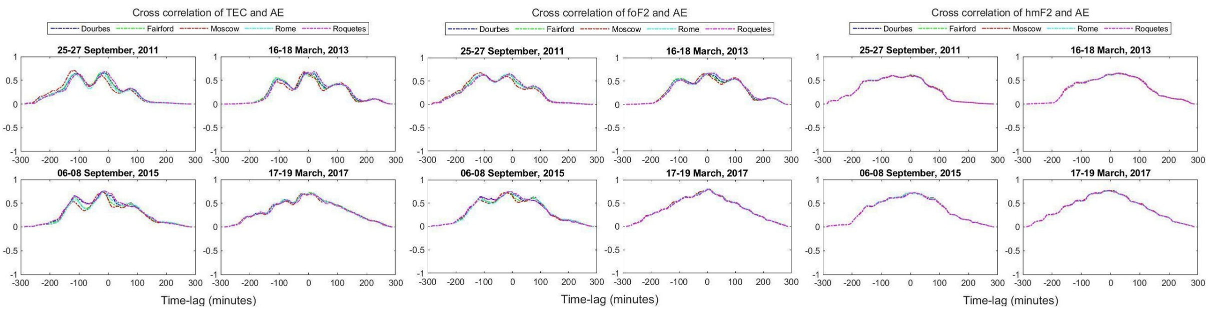

Figure 9: Cross-correlation of the ionospheric parameters with the AE index: TEC & AE (top), foF2 & AE (middle) and hmF2 & AE (bottom). In each block the panels are the storms of 25–27 September 2011 (1st), 16–18 March 2013 (2nd), 6–8 September 2015 (3rd) and the quiet days 18–20 March 2017 (4th). The x-axis is time lag (1 unit = 15 min); the y-axis is the correlation coefficient.

give statistical evidence of the pre-storm enhancement. But hmF2 always follows the storm indices at the same time and shows no such effect.

3.2 Discussion

The three events studied here give a common picture of the response of the mid-latitude ionosphere. The events with Sudden Storm Commencement (2011 and 2013) show a strong latitudinal dependence. The stations at higher latitude have lower values of Total Electron Content (TEC) and F2-region critical frequency (foF2), while the stations at lower latitude have higher values, as shown by [48] and [49]. This happens because of the decrease in the $n(O)/n(N_2)$ ratio at higher latitudes as suggested by [47]. The storm with gradual commencement (2015) did not show such dependence, as such storms are typically associated with high-speed streams from coronal holes and lack significant correlations with sunspot numbers and solar flares [58]. In all events, a positive storm trend initiated a day before the storm, persisted throughout the main phase, and diminished during the recovery phase. Despite Events 1 and 3 sharing the same seasonal conditions, the presence of an SSC in Event 1 and its absence in Event 3 led to distinct pre-storm enhancements, and Moscow, posi-

Table 2: Average of the highest cross-correlation values of all five stations in each storm event and their respective time lags. The values ranging from −1 to 1 represent normalized correlation coefficients, and 1 unit of time lag represents a time lag of 15 minutes

	2011	**2013**	**2015**
TEC & SYM/H	−0.573 at −30	−0.701 at −108.2	−0.736 at −32.8
foF2 & SYM/H	−0.640 at −127.6	−0.748 at −103.8	−0.734 at −27.2
hmF2 & SYM/H	−0.570 at −128.6	−0.795 at 0	−0.759 at 0
TEC & AE	0.679 at −55	0.665 at 0.8	0.749 at −17.6
foF2 & AE	0.635 at −16.6	0.658 at 3.8	0.737 at −14.4
hmF2 & AE	0.608 at −37.4	0.650 at 27.4	0.721 at 4.8

tioned at the highest latitude, experienced higher foF2 and TEC on the previous day than on the event day in Event 1, giving strong evidence of pre-storm enhancement. So, the strongest pre-storm effect is seen in the event which was caused by the most intense flare (X1.9), which hints that the pre-storm enhancement may depend on the intensity of the flare. However, the pre-storm phenomena are not caused by the magnetospheric electric fields, the disturbance dynamo electric fields or the solar flares alone. They rather point to a coupling mechanism between the interplanetary features and the thermosphere–ionosphere system, which continuously changes the dynamics, electrodynamics and chemistry of the ionosphere on a global scale before the arrival of the shock [37]. Energetic particles produced during flares and in fast ICME shocks can also penetrate deep into the atmosphere and affect the mid-latitude ionosphere within an hour up to four days after the flare [59]. So, the exact cause of these enhancements is still debatable.

The cross-correlation analysis gives numerical support to these findings. There is a robust correlation of the Symmetric-H and Auroral Electrojet indices with the ionospheric parameters, attributed to the coupling mechanism between the ionosphere and magnetosphere generating extreme electric field disturbances in middle–low-latitude regions. The cross-correlation of TEC and foF2 with the solar storm indices gives two stationary points of highest correlation, in which the ionospheric parameters lead the storm indices. This strongly suggests that the storm had its effect on the ionosphere at least a few hours before the main phase. But hmF2 correlates with the indices at nearly zero lag. The changes in TEC and foF2 can be positive or negative and they do not always agree with the seasons or with the phases of the storm [20]. This does not mean that there is a direct cause and effect relationship between the changes in TEC and foF2. Both of them have the geomagnetic disturbance as a common source. So, there is no doubt that the overall perturbations of the F2-layer parameters are caused by the geomagnetic storm. The mid-latitude ionosphere exhibits diverse, altitude- and region-dependent storm effects arising from multifaceted coupling processes [24,60]. The lead times obtained here and given in Table 2 are of a few hours to more than a day for TEC and foF2, while for hmF2 the lag is nearly zero. This shows that TEC and foF2 can be used as early indicators of a storm and hmF2 can be used as an indicator at the time of the storm. Such information is useful for monitoring and predicting the effects of geomagnetic storms on HF communication, GNSS positioning, satellite operation and the risk of geomagnetically induced currents in ground level conductor systems like power transmission lines.

Limitations of the study

This study has some limitations, which should be kept in mind while using the above results. First, the stations used here lie only in the European mid-latitude sector, so the results have to be tested for other longitudes and for the southern hemisphere. Second, only three storm events (two with SSC and one gradual) and one quiet time baseline are analyzed here, so the results are based on case studies and not on statistics of many events. Third, the ionogram parameters are scaled automatically, and such scaling has larger uncertainty during disturbed conditions even after manual checking. Fourth, cross-correlation gives the lead and lag time and the association between the parameters, but it does not prove the cause and effect. The separate contributions of the prompt penetration electric fields and of the disturbance dynamo have also not been isolated in this work. These points can be taken up in future work using a larger number of events and physics based models.

4 Conclusion

In this work, we have studied the cross-correlation of ionospheric parameters with the Symmetric-H and Auroral Electrojet indices during the geomagnetic storms of 25–27 September 2011, 16–18 March 2013, and 6–8 September 2015 over five European mid-latitude stations. It is observed that the values of Total Electron Content (TEC) and F2-region critical frequency (foF2) for the events with the presence of Sudden Storm Commencement (SSC) had a strong latitudinal dependence in the mid-latitude region, with stations at higher latitude having relatively lower values and those at lower latitudes having relatively higher values, while the event with gradual storm commencement showed no such dependence. The positive storm started a day before the events, remained so throughout the main phase, and then decreased during the recovery phase. The cross-correlation analysis of TEC and foF2 with the solar storm indices shows two stationary points of almost equal correlation magnitude, which strongly hints at the occurrence of pre-storm enhancement at least a few hours prior to the main phase of the geomagnetic storm, whereas the Maximum Ionization Height of the F2 layer (hmF2) showed no pre-storm effect, as its highest correlation with the storm indices occurred mostly at zero time lag.

A strong correlation of the Symmetric-H and Auroral Electrojet indices with the ionospheric parameters is observed, because the coupling mechanism between the ionosphere and magnetosphere produces extreme electric field disturbances in the middle–low-latitude regions. The highest correlation between the ionospheric parameters is mostly observed for Event 1 a day prior to the main phase. This might be because Event 1 was caused by the most intense solar flare (X1.9) among the selected events, which resulted in the strongest pre-storm effects. Events 1 and 3 have the same seasonal conditions, but their pre-storm enhancements are completely different. This is due to the nature of the two events, as Event 1 has SSC and Event 3 does not. Moscow, which is at the highest latitude, was affected by the pre-storm enhancement much more in Event 1 than in the other events. In practical terms, the storm-driven injection of solar-wind energy documented here, rapid electron-density fluctuations, Joule heating, particle precipitation, F2-layer uplift and TEC enhancements of up to ∼200% is precisely the chain that disturbs HF radio links, degrades GNSS accuracy, raises satellite drag, and drives geomagnetically induced currents in ground-level sensitive systems, including electric power transmission lines. The quantified lead times of TEC and foF2 relative to SYM/H and AE therefore provide a concrete observational basis for early-warning and mitigation strategies protecting both the upper-atmosphere segment and ground infrastructure from geomagnetic storm impacts.

Conflict of interests

The authors have no known or unknown financial or non-financial interests to disclose.

Acknowledgments

In this work, we have used the OMNIWeb service (http://omniweb.gsfc.nasa.gov/) for the interplanetary magnetic fields, solar wind parameters and geomagnetic indices. The Global Ionosphere Radio Observatory (GIRO, https://giro.uml.edu/) provided the ionospheric parameters. The station list was obtained from https://lgdc.uml.edu/common/DIDBFastStationList. The authors would like to thank them for the support provided.

References

[1] Gonzalez WD, Tsurutani BT. Criteria of interplanetary parameters causing intense magnetic storms (Dst < -100 nT). Planetary and Space Science. 1987;35(9):1101-9.

[2] Gonzalez W, Joselyn JA, Kamide Y, Kroehl HW, Rostoker G, Tsurutani B, et al. What is a geomagnetic storm? Journal of Geophysical Research: Space Physics. 1994;99(A4):5771-92.

[3] Gosling J. Coronal mass ejections: The link between solar and geomagnetic activity. Physics of Fluids B: Plasma Physics. 1993;5(7):2638-45.

[4] Gosling J. The solar flare myth in solar-terrestrial physics. Los Alamos National Laboratory, NM, United States; 1993.

[5] Bothmer V, Schwenn R. Eruptive prominences as sources of magnetic clouds in the solar wind. Space Science Reviews. 1994;70:215-20.

[6] Luhmann J. What do we really know about solar wind coupling? Advances in Space Research. 1997;20(4–5):907-11.

[7] Crooker N, McAllister A. Transients associated with recurrent storms. Journal of Geophysical Research: Space Physics. 1997;102(A7):14041-7.

[8] Kolawole M. Radar Systems, Peak Detection and Tracking. Oxford: Elsevier Science; 2003.

[9] Hargreaves JK. The Solar-Terrestrial Environment: An Introduction to Geospace — the Science of the Terrestrial Upper Atmosphere, Ionosphere, and Magnetosphere. Cambridge: Cambridge University Press; 1992.

[10] Sethi N, Pandey V. Comparative study of electron density from incoherent scatter measurements at Arecibo with the IRI-95 model during solar maximum. Annales Geophysicae. 2001;18:1630-4.

[11] Richards P. Seasonal and solar cycle variations of the ionospheric peak electron density: Comparison of measurement and models. Journal of Geophysical Research: Space Physics. 2001;106(A7):12803-19.

[12] Kawamura S, Balan N, Otsuka Y, Fukao S. Annual and semiannual variations of the midlatitude ionosphere under low solar activity. Journal of Geophysical Research: Space Physics. 2002;107(A8):1166.

[13] Liu J, Chen Y, Lin J. Statistical investigation of the saturation effect in the ionospheric foF2 versus sunspot, solar radio noise, and solar EUV radiation. Journal of Geophysical Research: Space Physics. 2003;108(A2):1067.

[14] Lei J, Liu L, Wan W, Zhang SR. Variations of electron density based on long-term incoherent scatter radar and ionosonde measurements over Millstone Hill. Radio Science. 2005;40(2):1-10.

[15] Liu L, Wan W, Ning B, Pirog O, Kurkin V. Solar activity variations of the ionospheric peak

electron density. Journal of Geophysical Research: Space Physics. 2006;111(A8):A08304.

[16] Zhang SR, Holt J. Ionospheric climatology and variability from long-term and multiple incoherent scatter radar observations: Variability. Annales Geophysicae. 2008;26:1525-37.

[17] Moen J, Qiu X, Carlson H, Fujii R, McCrea I. On the diurnal variability in F2-region plasma density above the EISCAT Svalbard radar. Annales Geophysicae. 2008;26:2427-33.

[18] Zhang ML, Liu C, Wan W, Liu L, Ning B. A global model of the ionospheric F2 peak height based on EOF analysis. Annales Geophysicae. 2009;27:3203-12.

[19] Souza J, Brum C, Abdu M, Batista I, Asevedo Jr W, Bailey G, et al. Parameterized regional ionospheric model and a comparison of its results with experimental data and IRI representations. Advances in Space Research. 2010;46(8):1032-8.

[20] Fuller-Rowell T, Codrescu M, Moffett R, Quegan S. Response of the thermosphere and ionosphere to geomagnetic storms. Journal of Geophysical Research: Space Physics. 1994;99(A3):3893-914.

[21] Volland H. Handbook of Atmospheric Electrodynamics. vol. 2. Boca Raton: CRC Press; 1995.

[22] Buonsanto MJ. Ionospheric storms — a review. Space Science Reviews. 1999;88(3):563-601.

[23] Mendillo M. Storms in the ionosphere: Patterns and processes for total electron content. Reviews of Geophysics. 2006;44(4):RG4001.

[24] Fagundes PR, Cardoso F, Fejer B, Venkatesh K, Ribeiro B, Pillat V. Positive and negative GPS-TEC ionospheric storm effects during the extreme space weather event of March 2015 over the Brazilian sector. Journal of Geophysical Research: Space Physics. 2016;121(6):5613-25.

[25] Blagoveshchensky DV, Sergeeva MA. Impact of geomagnetic storm of September 7–8, 2017 on ionosphere and HF propagation: A multi-instrument study. Advances in Space Research. 2019;63(1):239-56.

[26] Imtiaz N, Younas W, Khan M. Response of the low- to mid-latitude ionosphere to the geomagnetic storm of September 2017. Annales Geophysicae. 2020;38(2):359-72.

[27] Habarulema JB, Katamzi-Joseph ZT, Burešová D, Nndanganeni R, Matamba T, Tshisaphungo M, et al. Ionospheric response at conjugate locations during the 7–8 September 2017 geomagnetic storm over the Europe–African longitude sector. Journal of Geophysical Research: Space Physics. 2020;125(10):e2020JA028307.

[28] Atıcı R, Sagır S. Global investigation of the ionospheric irregularities during the severe geomagnetic storm on September 7–8, 2017. Geodesy and Geodynamics. 2020;11(3):211-21.

[29] Wang Z, Zou S, Liu L, Ren J, Aa E. Hemispheric asymmetries in the mid-latitude ionosphere during the September 7–8, 2017 storm: Multi-instrument observations. Journal of Geophysical Research: Space Physics. 2021;126(4):e2020JA028829.

[30] Themens DR, Elvidge S, McCaffrey A, Jayachandran PT, Coster A, Varney RH, et al. The high latitude ionospheric response to the major May 2024 geomagnetic storm: A synoptic view. Geophysical Research Letters. 2024;51(19):e2024GL111677.

[31] Sugiura M. Hourly values of equatorial Dst for the IGY. Annals of the International Geophysical Year. 1964;35:9-45.

[32] Rangarajan G. Indices of geomagnetic activity. In: Jacobs JA, editor. Geomagnetism. vol. 3. London: Academic Press; 1989. p. 323-84.

[33] Wanliss JA, Showalter KM. High-resolution global storm index: Dst versus SYM-H. Journal of Geophysical Research: Space Physics. 2006;111(A2):A02202.

[34] Blanc M, Richmond A. The ionospheric disturbance dynamo. Journal of Geophysical Research: Space Physics. 1980;85(A4):1669-86.

[35] Huang CS. Long-lasting penetration electric fields during geomagnetic storms: Observations and mechanisms. Journal of Geophysical Research: Space Physics. 2019;124(11):9640-64.

[36] Danilov A. F2-region response to geomagnetic disturbances. Journal of Atmospheric and Solar-Terrestrial Physics. 2001;63(5):441-9.

[37] Chukwuma VU. On ionospheric phenomena during pre-storm and main phase of a very intense geomagnetic storm. Acta Geophysica. 2010;58(6):1164-92.

[38] Reinisch BW, Huang X. Automatic calculation of electron density profiles from digital ionograms: 1. Automatic O and X trace identification for topside ionograms. Radio Science. 1982;17(2):421-34.

[39] Galkin IA, Reinisch BW. The new ARTIST 5 for all Digisondes. Ionosonde Network Advisory Group (INAG) Bulletin. 2008;69:1-8.

[40] Prölss G. Ionospheric F-region storms. In: Volland H, editor. Handbook of Atmospheric Electrodynamics. vol. 2. Boca Raton: CRC Press; 1995. p. 195-248.

[41] Astafyeva E, Zakharenkova I, Förster M. Ionospheric response to the 2015 St. Patrick's Day storm: A global multiinstrumental overview. Journal of Geophysical Research: Space Physics. 2015;120(10):9023-37.

[42] Marques de Souza A, Echer E, Bolzan MJA, Hajra R. Cross-correlation and cross-wavelet analyses of the solar wind IMF B_z and auroral electrojet index AE coupling during HILDCAAs. Annales Geophysicae. 2018;36:205-11.

[43] Pandit D, Chapagain NP, Adhikari B, et al. Analysis of the solar wind IMF B_z and auroral electrojet index during super substorms. Russian Journal of Earth Sciences. 2021;21(5):1-10.

[44] Foster J, Fairfield D, Ogilvie K, Rosenberg T. Relationship of interplanetary parameters and occurrence of magnetospheric substorms. Journal of Geophysical Research. 1971;76(28):6971-5.

[45] Adhikari B, Dahal S, Sapkota N, Baruwal P, Bhattarai B, Khanal K, et al. Field-aligned current and polar cap potential and geomagnetic disturbances: A review of crosscorrelation analysis. Earth and Space Science. 2018;5(9):440-55.

[46] Youssef M, Mahrous A, Mawad R, Ghamry E, Shaltout M, El-Nawawy M, et al. The effects of the solar magnetic polarity and the solar wind velocity on the Bz-component of the interplanetary magnetic field. Advances in Space Research. 2012;49(7):1198-202.

[47] Klimenko MV, Klimenko VV, Zakharenkova IE, Ratovsky KG, Korenkova NA, Yasyukevich YV, et al. Similarity and differences in morphology and mechanisms of the foF2 and TEC disturbances during the geomagnetic storms on 26–30 September 2011. Annales Geophysicae. 2017;35:923-38.

[48] Liu W, Xu L, Xiong C, Xu J. The ionospheric storms in the American sector and their longitudinal dependence at the northern middle latitudes. Advances in Space Research. 2017;59(2):603-13.

[49] Gao Q, Liu LB, Zhao BQ, Wan WX, Zhang ML, Ning BQ. Statistical study of the storm effects in middle and low latitude ionosphere in the East-Asian sector. Chinese Journal of Geophysics. 2008;51(3):435-43.

[50] Prölss G, Ocko M. Propagation of upper atmospheric storm effects towards lower latitudes. Advances in Space Research. 2000;26(1):131-5.

[51] Baker D, Jaynes A, Li X, Henderson M, Kanekal S, Reeves G, et al. Gradual diffusion and punctuated phase space density enhancements of highly relativistic electrons: Van Allen Probes observations. Geophysical Research Letters. 2014;41(5):1351-8.

[52] Verkhoglyadova O, Tsurutani B, Mannucci A, Mlynczak M, Hunt L, Paxton L, et al. Solar wind driving of ionosphere-thermosphere responses in three storms near St. Patrick's Day in 2012, 2013, and 2015. Journal of Geophysical Research: Space Physics. 2016;121(9):8900-23.

[53] Lugaz N, Farrugia CJ, Smith CW, Paulson K. Shocks inside CMEs: A survey of properties from 1997 to 2006. Journal of Geophysical Research: Space Physics. 2015;120(4):2409-27.

[54] Du A, Tsurutani B, Sun W. Solar wind energy input during prolonged, intense northward interplanetary magnetic fields: A new coupling function. Journal of Geophysical Research: Space Physics. 2011;116(A12):A12215.

[55] Sibeck D. A model for the transient magnetospheric response to sudden solar wind dynamic pressure variations. Journal of Geophysical Research: Space Physics. 1990;95(A4):3755-71.

[56] Adekoya B, Chukwuma V, Bakare N, David T. On the effects of geomagnetic storms and pre-storm phenomena on low and middle latitude ionospheric F2. Astrophysics and Space Science. 2012;340(2):217-35.

[57] Xiong C, Lühr H, Wang H, Johnsen MG. Determining the boundaries of the auroral oval from CHAMP field-aligned current signatures — Part 1. Annales Geophysicae. 2014;32:609-22.

[58] Veretenenko S, Ogurtsov M, Obridko V. Geophysical effects of solar activity: long-term variations in occurrences of magnetic storms with sudden and gradual commencements. Journal of Physics: Conference Series. 2019;1400:022038.

[59] Tsurutani B, Verkhoglyadova O, Mannucci A, Lakhina G, Li G, Zank G. A brief review of "solar flare effects" on the ionosphere. Radio Science. 2009;44(1):RS0A17.

[60] Meloni A, De Michelis P, Tozzi R. Geomagnetic storms, dependence on solar and interplanetary phenomena: a review. Memorie della Società Astronomica Italiana. 2005;76:882-7.